Journal of Sound and Vibration (2001) **240**(5), 891–908
doi:10.1006/jsvi.2000.3258, available online at http://www.idealibrary.com on IDEAL®

VIBRATION ANALYSIS OF ROTATING PRE-TWISTED BLADES WITH A CONCENTRATED MASS

H. H. Yoo

School of Mechanical Engineering, Hanyang University, Sungdong-Gu Haengdang-Dong 17, *Seoul* 133-791, *Republic of Korea. E-mail: hhyoo@email.hanyang.ac.kr*

J. Y. Kwak

Samsung Commercial Vehicles Co., Ltd., Dalseo-Gu Pasan-Dong, Daegu 704-230, *Republic of Korea*

AND

J. Chung

Department of Mechanical Engineering, Hanyang University, 1271 *Sa*-1-*Dong, Ansan, Kyunggi-Do* 425-791, *Republic of Korea*

(*Received* 28 *July* 1999, *and in final form* 1 *August* 2000)

A modelling method for the vibration analysis of rotating pretwisted blades with a concentrated mass is presented in this paper. The blade has an arbitrary orientation with respect to the rigid hub to which it is fixed. The equations of motion are derived based on a modelling method that employs hybrid deformation variables. The resulting equations for the vibration analysis are transformed into a dimensionless form in which dimensionless parameters are identified. The effects of the dimensionless parameters on the modal characteristics of the rotating blade are investigated through numerical analysis.

1. INTRODUCTION

Structures having the shape of blades are often found in several practical engineering examples such as turbines and aircraft rotary wings. For reliable and economic designs of the structures, it is necessary to estimate the modal characteristics of those structures accurately. Since significant variations of modal characteristics result from rotational motion of the structures, they have been investigated by many researchers.

An early analytical model to calculate natural frequencies of a rotating beam was suggested in reference [1]. Based on the Rayleigh energy theorem, a simple equation that related the natural frequency to the rotating frequency of a beam was suggested. This equation is well known as Southwell equation, and widely used by many engineers even nowadays. Later, to obtain more accurate natural frequencies, a linear partial differential equation that governs bending vibration of a rotating beam was derived (see reference [2]). Applying Ritz method to the equation, more accurate coefficients for the Southwell equation could be obtained. Since early 1970s, due to the astonishing progress of computing technologies, large number of papers based on numerical approaches have been published. For instance, in reference [3, 4], approximation methods for the modal analysis of rotating beams were employed. More complex shapes and effects of beams were considered, too. The effects of tip mass (see reference [5, 6]), elastic foundation and cross-section variation

0022-460X/01/100891 + 18 $35.00/0

(see reference [7]), shear deformation (see reference [8]), the pre-twist and the orientation of the blade (see reference [9]), and the gyroscopic damping effect (see reference [10]) on the modal characteristics of rotating beams were studied. Survey papers (see reference [11, 12]) in which large number of related papers are reviewed are available, too.

In this study, a model to analyze the vibration characteristics of a rotating blade is presented. The effects of a concentrated mass as well as its arbitrary location, the pre-twist angle, and the orientation of the blade are incorporated into the model. In previous studies (see reference [5, 6, 9, 13]), these effects have not been considered simultaneously, and the concentrated mass is located at the tip of the blade. To obtain the equations of motion, a modelling method using hybrid deformation variables is employed. The use of hybrid deformation variables is the key ingredient to capture the stiffness variation due to rotational motion. Linear equations of motion are derived directly based on Kane's method (see reference [14]). The validity of the modelling method that employs hybrid deformation variables was verified in reference [15]. To draw general conclusions from numerical results, the equations of motion are transformed into dimensionless forms by using dimensionless variables. Dimensionless parameters corresponding to the concentrated mass, the location of the concentrated mass, the angular speed, the hub radius, the principal area moment of inertia ratio, the pre-twist angle, and the orientation angles are identified. The effects of these parameters on the modal characteristics of the rotating blade are investigated in this study.

2. EQUATIONS OF MOTION

2.1. SYSTEM CONFIGURATION

The following assumptions are made in this study: the blade has homogeneous and isotropic material property. The pre-twist rate of the blade along its longitudinal axis is uniform. The blade has slender shape so that shear and rotary inertia effects will be neglected. The neutral and centroidal axes in the cross-section of the blade coincide so that eccentricity effect will not be considered. No external force acts on the blade.

Figure 1 shows the configuration of a pre-twisted blade. θ_0 is the pretwisted angle of the free end (to which $\hat{b}_1$, $\hat{b}_2$, and $\hat{b}_3$ are attached) with respect to the fixed end (to which $\hat{a}_1$, $\hat{a}_2$, and $\hat{a}_3$ are attached). Thus, $\hat{b}_1 = \hat{a}_1$ and $\cos\theta_0 = \hat{a}_2 \cdot \hat{b}_2$.

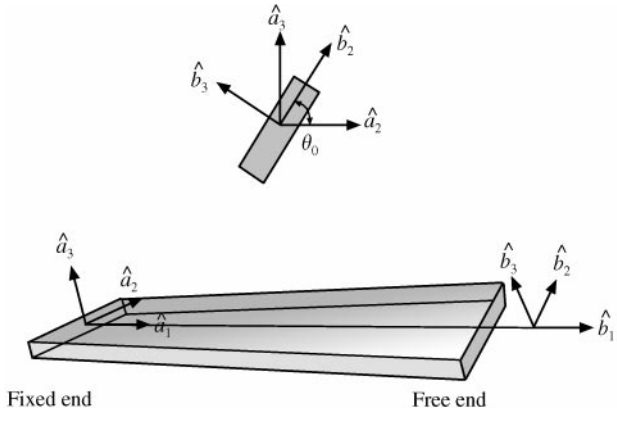

Figure 1. Configuration of a pre-twisted blade.

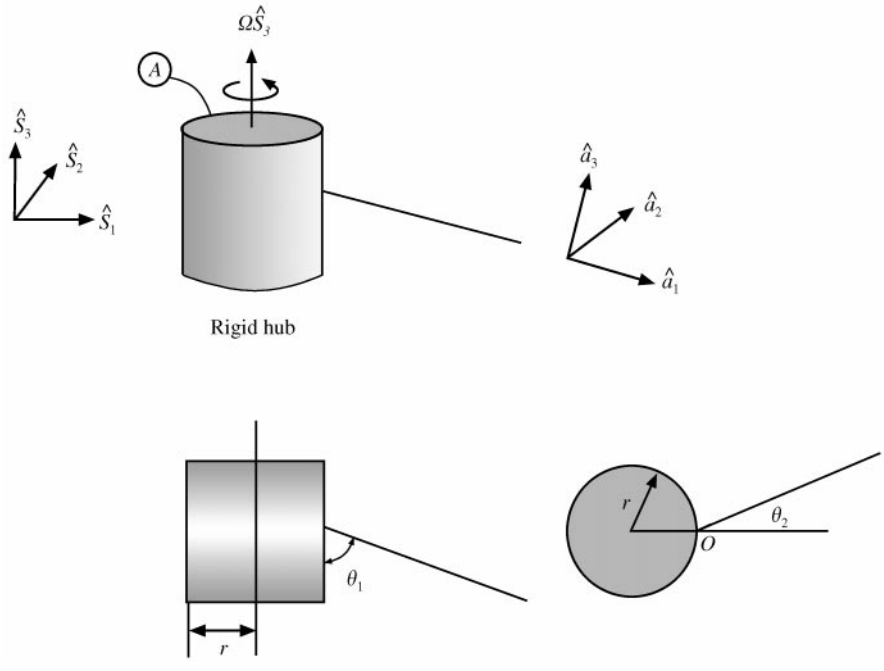

Figure 2. Orientation of the undeformed blade neutral axis.

Figure 2 shows the undeformed configuration of the blade neutral axis which has an arbitrary orientation with respect to the rigid hub. Mutually, orthogonal unit vectors $\hat{s}_1$, $\hat{s}_2$, and $\hat{s}_3$ are fixed to the rigid hub A which rotates with angular velocity $\Omega\hat{s}_3$. The orientation of the blade neutral axis can be defined by taper angle θ_1 (rotation about $\hat{s}_2$), eccentric angle θ_2 (rotation about $\hat{s}_3$), and the setting angle (rotation about $\hat{s}_1$). The eccentric angle, if considered here in the formulation, is not usually allowed for the design of a blade since it introduces extremely large bending stress during the rotation. Moreover, the setting angle is not considered here since its effect can be included by changing the area moments and products of inertia of the blade cross-section. For the convenience of describing deformation vectors, another unit vector triad ($\hat{a}_1$, $\hat{a}_2$, and $\hat{a}_3$), which is also fixed to the rigid hub A, is shown in the figure.

Figure 3 shows the deformation of the blade neutral axis. A concentrated mass is located at an arbitrary position of the neutral axis. P_0 and P are the positions of a generic point before and after deformation respectively. Conventionally, only Cartesian variables are employed to describe the deformation. In the present modelling method, however, a non-Cartesian variable s denoting the arc length stretch of the neutral axis is employed. There is a geometric relation between the arc length stretch and the Cartesian variables (see references [15]). Since the arc length stetch s instead of u_1 is approximated in this study, this geometric relation is used to derive generalized inertia forces in the equations of motion. Since linear equations of motion are to be derived eventually, the following approximate relationship is used:

$$s = u_1 + \frac{1}{2}\int_0^x \left[\left(\frac{\partial u_2}{\partial \sigma}\right)^2 + \left(\frac{\partial u_3}{\partial \sigma}\right)^2\right] \mathrm{d}\sigma. \tag{1}$$

The use of the above approximate equation significantly simplifies the procedure of deriving the equations of motion.

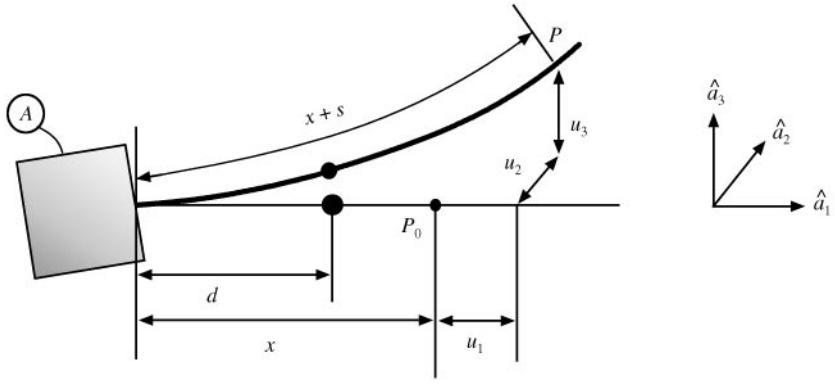

Figure 3. Deformation of the blade neutral axis and the location of a concentrated mass.

2.2. APPROXIMATION AND STRAIN ENERGY

In the present modelling method, s, u_2 and u_3 are approximated by using spatial functions and corresponding co-ordinates in order to derive the ordinary differential equations of motion. The Rayleigh–Ritz method is employed to approximate the variables as follows:

$$s(x, t) = \sum_{i=1}^{\mu_1} \phi_{1i}(x) q_{1i}(t), \tag{2}$$

$$u_2(x, t) = \sum_{i=1}^{\mu_2} \phi_{2i}(x) q_{2i}(t), \tag{3}$$

$$u_3(x, t) = \sum_{i=1}^{\mu_3} \phi_{3i}(x) q_{3i}(t), \tag{4}$$

where ϕ_{1i}, ϕ_{2i}, and ϕ_{3i} are the spatial functions for s, u_2 and u_3; q_{1i}, q_{2i}, and q_{3i} are corresponding generalized co-ordinates; and μ_1, μ_2, and μ_3 are the numbers of respective generalized co-ordinates.

Using the arc length stretch, the strain energy can be expressed as follows:

$$U = \frac{1}{2}\int_0^L \left[EA\left(\frac{\partial s}{\partial x}\right)^2 + EI_3\left(\frac{\partial^2 u_2}{\partial x^2}\right)^2 + EI_2\left(\frac{\partial^2 u_3}{\partial x^2}\right)^2 + 2EI_{23}\left(\frac{\partial^2 u_2}{\partial x^2}\right)\left(\frac{\partial^2 u_3}{\partial x^2}\right)\right] \mathrm{d}x, \tag{5}$$

where E denotes Young's modulus, A is the cross-sectional area of the blade, I_2, I_3 and I_{23} are second area moments and product of inertia of the cross-section, and L is the undeformed length of the blade. By using I_2^* and I_3^*, the principal second area moments of the cross-section, I_2, I_3 and I_{23} can be expressed as follows:

$$I_2(x) = \frac{I_2^* + I_3^*}{2} + \frac{I_2^* - I_3^*}{2}\cos(2\theta), \tag{6}$$

$$I_3(x) = \frac{I_2^* + I_3^*}{2} + \frac{I_2^* - I_3^*}{2}\cos(2\theta), \tag{7}$$

$$I_{23}(x) = \frac{I_2^* - I_3^*}{2}\sin(2\theta), \tag{8}$$

where

$$\theta \equiv \theta_0 \frac{x}{L}, \tag{9}$$

θ is the pre-twist angle of a cross-section with respect to the fixed end. Thus, $\theta = 0$ at the fixed end, and $\theta = \theta_0$ at the free end.

2.3. EQUATIONS OF MOTION

With the assumptions given in section 2.1, the equations of motion can be obtained from the following equation (see reference [14]):

$$\int_0^L \rho \mathbf{a}^P \cdot \left(\frac{\partial \mathbf{v}^P}{\partial \dot{q}_i} \right) \mathrm{d}x + \frac{\partial U}{\partial q_i} = 0 \quad (i = 1, 2, \ldots, \mu), \tag{10}$$

where ρ is the mass per unit length of the blade, q_i's consist of the generalized co-ordinates q_{1i}, q_{2i}, and q_{3i}; and $\mathbf{v}^P$ and $\mathbf{a}^P$ are the velocity and the acceleration of the generic point P respectively. The acceleration can be obtained simply by differentiating the velocity $\mathbf{v}^P$ with respect to time, which can be obtained by using the following equation:

$$\mathbf{v}^P = \mathbf{v}^O + \frac{{}^A\mathrm{d}\mathbf{p}}{\mathrm{d}t} + \boldsymbol{\omega}^A \times \mathbf{p}, \tag{11}$$

where $\mathbf{v}^O$ is the velocity of point O that is fixed to the rigid hub, $\boldsymbol{\omega}^A$ is the angular velocity of the rigid hub, and $\mathbf{p}$ is the vector from point O to point P. The second term on the right-hand side of equation (11) denotes the time differentiation of vector $\mathbf{p}$ in the reference frame A. Using the co-ordinate systems fixed to the rigid hub, $\mathbf{v}^O$, $\boldsymbol{\omega}^A$, and $\mathbf{p}$ can be expressed as follows:

$$\mathbf{v}^O = r\Omega \hat{s}_2, \qquad \boldsymbol{\omega}^A = \Omega \hat{s}_3, \tag{12, 13}$$

$$\mathbf{p} = (x + u_1)\hat{a}_1 + u_2\hat{a}_2 + u_3\hat{a}_3, \tag{14}$$

where r is the radius of the rigid hub and Ω is the angular speed of the rigid hub (see Figure 2). Since the blade has arbitrary orientation with respect to the rigid hub, the two co-ordinate systems ($\hat{s}_1$, $\hat{s}_2$, $\hat{s}_3$ and $\hat{a}_1$, $\hat{a}_2$, $\hat{a}_3$) have the following relationship:

$$\hat{s}_1 = c_{11}\hat{a}_1 + c_{12}\hat{a}_2 + c_{13}\hat{a}_3, \tag{15}$$

$$\hat{s}_2 = c_{21}\hat{a}_1 + c_{22}\hat{a}_2 + c_{23}\hat{a}_3, \tag{16}$$

$$\hat{s}_3 = c_{31}\hat{a}_1 + c_{32}\hat{a}_2 + c_{33}\hat{a}_3, \tag{17}$$

where c_{ij} represent the direction cosines between $\hat{s}_i$ and $\hat{a}_j$ which can be easily obtained by using the taper angle θ_1 and the eccentric angle θ_2. Space 1-2-3 Euler angles are employed in this study. The taper angle is the second Euler angle and the eccentric angle is the third Euler angle. The first Euler angle is set to 0. Thus,

$$\begin{aligned} &c_{11} = \cos\theta_1 \cos\theta_2, \qquad c_{12} = -\sin\theta_2, \qquad c_{13} = \sin\theta_1 \cos\theta_2, \\ &c_{21} = \cos\theta_1 \sin\theta_2, \qquad c_{22} = \cos\theta_2, \qquad c_{23} = \sin\theta_1 \sin\theta_2, \\ &c_{31} = -\sin\theta_1, \qquad c_{32} = 0, \qquad c_{33} = \cos\theta_1 . \end{aligned} \tag{18}$$

Now, by using equations (11)–(17), the velocity of point P can be obtained as follows:

$$\begin{aligned}\mathbf{v}^P = &\{r\Omega c_{21} + \dot{u}_1 + \Omega(c_{32}u_3 - c_{33}u_2)\}\,\hat{a}_1 \\ &+ \{r\Omega c_{22} + \dot{u}_2 + \Omega[c_{33}(x+u_1) - c_{31}u_3]\}\,\hat{a}_2 \\ &+ [r\Omega c_{23} + \dot{u}_3 + \Omega[c_{31}u_2 - c_{32}(x+u_1)]\}\,\hat{a}_3.\end{aligned} \tag{19}$$

To derive the equations of motion by employing Kane's method, the partial derivatives of the velocity of P with respect to the generalized speed $\dot{q}_i$'s are to be obtained. Thus,

$$\frac{\partial \mathbf{v}^P}{\partial \dot{q}_{1i}} = \phi_{1i}\hat{a}_1 \quad (i = 1, 2, \dots, \mu_1), \tag{20}$$

$$\frac{\partial \mathbf{v}^P}{\partial \dot{q}_{2i}} = \left[-\sum_{j=1}^{\mu_2} \left(\int_0^x \phi'_{2i}\phi'_{2j}\,\mathrm{d}\sigma \right) q_{2j} \right] \hat{a}_1 + \phi_{2i}\hat{a}_2 \quad (i = 1, 2, \dots, \mu_2), \tag{21}$$

$$\frac{\partial \mathbf{v}^P}{\partial \dot{q}_{3i}} = \left[-\sum_{j=1}^{\mu_3} \left(\int_0^x \phi'_{3i}\phi'_{3j}\,\mathrm{d}\sigma \right) q_{3j} \right] \hat{a}_1 + \phi_{3i}\hat{a}_3 \quad (i = 1, 2, \dots, \mu_3), \tag{22}$$

where a symbol with a prime ($'$) represents the partial derivative of the symbol with respect to the integral domain variable. By using equation (1)–(22), the linearized equations of motion are obtained as follows:

$$\sum_{j=1}^{\mu_1} M_{ij}^{11}\,\ddot{q}_{1j} + \sum_{j=1}^{\mu_1} \{K_{ij}^S - (c_{32}^2 + c_{33}^2)\Omega^2 M_{ij}^{11}\}\,q_{1j} + \sum_{j=1}^{\mu_2} (c_{32}c_{31}\Omega^2 M_{ij}^{12} q_{2j} - 2c_{33}\Omega M_{ij}^{12}\dot{q}_{2j}) \tag{23}$$

$$+ \sum_{j=1}^{\mu_3} (c_{33}c_{31}\Omega^2 M_{ij}^{13} q_{3j} + 2c_{32}\Omega M_{ij}^{13}\dot{q}_{3j}) = r(c_{33}c_{22} - c_{32}c_{23})\Omega^2 P_{1i} + (c_{32}^2 + c_{33}^2)\Omega^2 Q_{1i},$$

$$\sum_{j=1}^{\mu_2} M_{ij}^{22}\,\ddot{q}_{2j} + 2c_{33}\Omega \sum_{j=1}^{\mu_1} M_{ij}^{21}\,\dot{q}_{1j} + \sum_{j=1}^{\mu_3} (K_{ij}^{B23} + c_{33}c_{32}\Omega^2 M_{ij}^{23})\,q_{3j}$$

$$- 2c_{31}\Omega \sum_{j=1}^{\mu_3} M_{ij}^{23}\dot{q}_{3j} + c_{31}c_{32}\,\Omega^2 \sum_{j=1}^{\mu_1} M_{ij}^{21} q_{1j} \tag{24}$$

$$+ \sum_{j=1}^{\mu_2} \{(c_{32}^2 + c_{33}^2)\Omega^2 K_{ij}^{GB2} - r(c_{32}c_{23} - c_{33}c_{22})\Omega^2 K_{ij}^{GA2} + K_{ij}^{B2} - (c_{33}^2 + c_{31}^2)\Omega^2 M_{ij}^{22}\}\,q_{2j}$$

$$= r(c_{31}c_{23} - c_{33}c_{21})\Omega^2 P_{2i} - c_{31}c_{32}\Omega^2 Q_{2i},$$

$$\sum_{j=1}^{\mu_3} M_{ij}^{33}\,\ddot{q}_{3j} + 2c_{31}\Omega \sum_{j=1}^{\mu_2} M_{ij}^{32}\dot{q}_{2j} + \sum_{j=1}^{\mu_2} (K_{ij}^{B32} + c_{32}c_{33}\Omega^2 M_{ij}^{32})\,q_{2j}$$

$$- 2c_{32}\Omega \sum_{j=1}^{\mu_1} M_{ij}^{31}\dot{q}_{1j} + c_{31}c_{33}\,\Omega^2 \sum_{j=1}^{\mu_1} M_{ij}^{31} q_{1j} \tag{25}$$

$$+ \sum_{j=1}^{\mu_3} \{(c_{32}^2 + c_{33}^2)\Omega^2 K_{ij}^{GB3} - r(c_{32}c_{23} - c_{33}c_{22})\Omega^2 K_{ij}^{GA3} + K_{ij}^{B3} - (c_{31}^2 + c_{32}^2)\Omega^2 M_{ij}^{33}\}\,q_{3j}$$

$$= r(c_{32}c_{21} - c_{31}c_{22})\Omega^2 P_{3i} - c_{31}c_{33}\Omega^2 Q_{3i},$$

where

$$M_{ij}^{ab} \equiv \int_0^L \rho \phi_{ai} \phi_{bj} \, \mathrm{d}x, \tag{26}$$

$$K_{ij}^{GAa} \equiv \int_0^L \rho (L - x) \phi'_{ai} \phi'_{aj} \, \mathrm{d}x, \tag{27}$$

$$K_{ij}^{GBa} \equiv \int_0^L \frac{\rho}{2} (L^2 - x^2) \phi'_{ai} \phi'_{aj} \, \mathrm{d}x, \tag{28}$$

$$P_{ai} \equiv \int_0^L \rho \phi_{ai} \, \mathrm{d}x, \tag{29}$$

$$Q_{ai} \equiv \int_0^L \rho x \phi_{ai} \, \mathrm{d}x, \tag{30}$$

$$K_{ij}^{S} \equiv \int_0^L EA \phi'_{1i} \phi'_{1j} \, \mathrm{d}x, \tag{31}$$

$$K_{ij}^{B2} \equiv \int_0^L EI_3 \phi''_{2i} \phi''_{2j} \, \mathrm{d}x, \tag{32}$$

$$K_{ij}^{B3} \equiv \int_0^L EI_2 \phi''_{3i} \phi''_{3j} \, \mathrm{d}x, \tag{33}$$

$$K_{ij}^{Bab} \equiv \int_0^L EI_{23} \phi''_{ai} \phi''_{bj} \, \mathrm{d}x, \tag{34}$$

a symbol with a double prime ($''$) represents the double differentiation of the symbol with respect to the integral domain variable.

Expressing the mass per unit length of the blade by using a Dirac's delta function enables us to consider a concentrated mass at an arbitrary location of the blade (for instance, at $x = d$ as shown in Figure 3).

$$\rho^*(x) = \rho(x) + m\delta(x - d), \tag{35}$$

where m is the magnitude of the concentrated mass. Substituting ρ^* for ρ into equation (26)–(30), the integral values of equations (26)–(30) can be obtained as follows:

$$\widehat{M_{ij}^{ab}} \equiv M_{ij}^{ab} + m\phi_{ai}(d)\phi_{bj}(d), \tag{36}$$

$$\widehat{K_{ij}^{GAa}} \equiv K_{ij}^{GAa} + m \int_0^d \phi'_{ai} \phi'_{aj} \, \mathrm{d}x, \tag{37}$$

$$\widehat{K_{ij}^{GBa}} \equiv K_{ij}^{GBa} + md \int_0^d \phi'_{ai} \phi'_{aj} \, \mathrm{d}x, \tag{38}$$

$$\widehat{P_{ai}} \equiv P_{ai} + m\phi_{ai}(d), \tag{39}$$

$$\widehat{Q_{ai}} \equiv Q_{ai} + md\phi_{ai}(d). \tag{40}$$

The coupling effect between the stretching and the bending motions will be neglected in this study. It was proved (see reference [10]) that the coupling effect can be ignored for slender beams. Ignoring the coupling effect and stretching equations, the equations of motion of the blade can be simplified as follows:

$$\sum_{j=1}^{\mu_2} \widehat{M_{ij}^{22}}\,\ddot{q}_{2j} - 2c_{31}\Omega \sum_{j=1}^{\mu_3} \widehat{M_{ij}^{23}}\,\dot{q}_{3j} + \sum_{j=1}^{\mu_3} (K_{ij}^{B23} + c_{33}c_{32}\Omega^2 \widehat{M_{ij}^{23}})q_{3j}$$
$$+ \sum_{j=1}^{\mu_2} \{(c_{32}^2 + c_{33}^2)\Omega^2 \widehat{K_{ij}^{GB2}} - r(c_{32}c_{23} - c_{33}c_{22})\Omega^2 \widehat{K_{ij}^{GA2}} + K_{ij}^{B2}$$
$$- (c_{33}^2 + c_{31}^2)\Omega^2 \widehat{M_{ij}^{22}}\}\, q_{2j} = r(c_{31}c_{23} - c_{33}c_{21})\Omega^2 \widehat{P_{2i}} - c_{31}c_{32}\Omega^2 \widehat{Q_{2i}}, \tag{41}$$

$$\sum_{j=1}^{\mu_3} \widehat{M_{ij}^{33}}\,\ddot{q}_{3j} + 2c_{31}\Omega + \sum_{j=1}^{\mu_2} \widehat{M_{ij}^{32}}\,\dot{q}_{2j} + \sum_{j=1}^{\mu_2} (K_{ij}^{B32} + c_{32}c_{33}\Omega^2 \widehat{M_{ij}^{32}})q_{2j}$$
$$+ \sum_{j=1}^{\mu_3} \{(c_{32}^2 + c_{33}^2)\Omega^2 \widehat{K_{ij}^{GB3}} - r(c_{32}c_{23} - c_{33}c_{22})\Omega^2 K_{ij}^{GA3} + K_{ij}^{B3}$$
$$- (c_{31}^2 + c_{32}^2)\Omega^2 \widehat{M_{ij}^{33}}\}\, q_{3j} = r(c_{32}c_{21} - c_{31}c_{22})\Omega^2 \widehat{P_{3i}} - c_{31}c_{33}\Omega^2 \widehat{Q_{3i}}. \tag{42}$$

2.4. DIMENSIONLESS EQUATIONS OF MOTION

To draw general conclusions from numerical results, equation (41) and (42) are to be transformed into dimensionless equations. For this transformation, dimensionless variables and parameters need to be defined as follows:

$$\tau \equiv \frac{t}{T}, \qquad \xi \equiv \frac{x}{L}, \qquad \vartheta_{ai} \equiv \frac{q_{ai}}{L}, \tag{43–45}$$

$$\alpha \equiv \frac{m}{\rho L}, \qquad \beta \equiv \frac{d}{L}, \qquad \gamma \equiv \Omega T, \tag{46–48}$$

$$\delta \equiv \frac{r}{L}, \qquad \kappa \equiv \frac{I_2^*}{I_3^*}, \tag{49, 50}$$

where T appearing in equation (43) and (48) is defined as

$$T \equiv \sqrt{\frac{\rho L^4}{E I_3^*}}. \tag{51}$$

Hereinafter, α, β, γ, δ, κ will be called concentrated mass ratio, concentrated mass location ratio, angular speed ratio, hub radius ratio, and principal area moment of inertia ratio respectively. By using the parameter defined in equation (50), equation (4)–(6) can be expressed as

$$\frac{I_2}{I_3^*} = \tfrac{1}{2}(\kappa + 1) + \tfrac{1}{2}(\kappa - 1)\cos(2\theta_0 \xi), \tag{52}$$

$$\frac{I_3}{I_3^*} = \tfrac{1}{2}(\kappa + 1) - \tfrac{1}{2}(\kappa - 1)\cos(2\theta_0 \xi), \tag{53}$$

$$\frac{I_{23}}{I_3^*} = \tfrac{1}{2}(\kappa - 1)\sin(2\theta_0\xi). \tag{54}$$

The right-hand side terms in equation (41) and (42) may be neglected for the free vibration analysis. By using the dimensionless variables and parameters defined in equation (43)–(50), the dimensionless equations of motion are finally obtained as follows:

$$\sum_{j=1}^{\mu_2} \bar{M}_{ij}^{22}\,\ddot{\vartheta}_{2j} - 2c_{31}\gamma \sum_{j=1}^{\mu_3} \bar{M}_{ij}^{23}\,\dot{\vartheta}_{3j} + \sum_{j=1}^{\mu_3} (\bar{K}_{ij}^{B23} + c_{33}c_{32}\gamma^2 \bar{M}_{ij}^{23})\,\vartheta_{3j}$$

$$+ \sum_{j=1}^{\mu_2} \{(c_{32}^2 + c_{33}^2)\gamma^2(\bar{K}_{ij}^{GB2} + \alpha\beta\bar{K}_{ij}^{GC2}) - \delta\gamma^2(c_{32}c_{23} - c_{33}c_{22})(\bar{K}_{ij}^{GA2} + \alpha\bar{K}_{ij}^{GC2})$$

$$+ \bar{K}_{ij}^{B2} - (c_{33}^2 + c_{31}^2)\gamma^2\bar{M}_{ij}^{22}\}\,\vartheta_{2j} = 0, \tag{55}$$

$$\sum_{j=1}^{\mu_3} \bar{M}_{ij}^{33}\,\ddot{\vartheta}_{3j} + 2c_{31}\gamma \sum_{j=1}^{\mu_2} \bar{M}_{ij}^{32}\,\dot{\vartheta}_{2j} + \sum_{j=1}^{\mu_2} (\bar{K}_{ij}^{B23} + c_{32}c_{33}\gamma^2 \bar{M}_{ij}^{32})\,\vartheta_{2j}$$

$$+ \sum_{j=1}^{\mu_3} \{(c_{32}^2 + c_{33}^2)\gamma^2(\bar{K}_{ij}^{GB3} + \alpha\beta\bar{K}_{ij}^{GC3}) - \delta\gamma^2(c_{32}c_{23} - c_{33}c_{22})(\bar{K}_{ij}^{GA3} + \alpha\bar{K}_{ij}^{GC3})$$

$$+ \bar{K}_{ij}^{B3} - (c_{31}^2 + c_{32}^2)\gamma^2\bar{M}_{ij}^{33}\}\,\vartheta_{3j} = 0, \tag{56}$$

where

$$\bar{M}_{ij}^{ab} \equiv \int_0^1 \psi_{ai}\psi_{bj}\,\mathrm{d}\xi + \alpha\psi_{ai}(\beta)\psi_{bj}(\beta), \tag{57}$$

$$\bar{K}_{ij}^{B2} \equiv \int_0^1 \left\{\frac{1}{2}(\kappa + 1) - \frac{1}{2}(\kappa - 1)\cos(2\theta_0\xi)\right\}\psi_{2i}''\psi_{2j}''\,\mathrm{d}\xi, \tag{58}$$

$$\bar{K}_{ij}^{B3} \equiv \int_0^1 \left\{\frac{1}{2}(\kappa + 1) + \frac{1}{2}(\kappa - 1)\cos(2\theta_0\xi)\right\}\psi_{3i}''\psi_{3j}''\,\mathrm{d}\xi, \tag{59}$$

$$\bar{K}_{ij}^{GAa} \equiv \int_0^1 (1 - \xi)\psi_{ai}'\psi_{aj}'\,\mathrm{d}\xi, \tag{60}$$

$$\bar{K}_{ij}^{GBa} \equiv \int_0^1 \frac{1}{2}(1 - \xi^2)\psi_{ai}'\psi_{aj}'\,\mathrm{d}\xi, \tag{61}$$

$$\bar{K}_{ij}^{GCa} \equiv \int_0^\beta \psi_{ai}'\psi_{aj}'\,\mathrm{d}\xi, \tag{62}$$

$$\bar{K}_{ij}^{Bab} \equiv \int_0^1 \frac{1}{2}(\kappa - 1)\sin(2\theta_0\xi)\,\psi_{ai}''\psi_{bj}''\,\mathrm{d}\xi, \tag{63}$$

where ψ, which is equivalent to ϕ, is a function of ξ.

2.5. MODAL FORMULATION

Equations (55) and (56) are expressed in a matrix form as follows:

$$\mathbf{M}\ddot{\vartheta} + \mathbf{C}\dot{\vartheta} + \mathbf{K}\vartheta = \mathbf{0}, \tag{64}$$

where

$$\mathbf{M} \equiv \begin{bmatrix} \bar{M}^{22} & 0 \\ 0 & \bar{M}^{33} \end{bmatrix}, \qquad \mathbf{C} \equiv \begin{bmatrix} 0 & -c_{31}\bar{M}^{23} \\ c_{31}\bar{M}^{32} & 0 \end{bmatrix}, \tag{65, 66}$$

$$\mathbf{K} \equiv \begin{bmatrix} \bar{K}^{22} & \bar{K}^{23} \\ \bar{K}^{32} & \bar{K}^{33} \end{bmatrix}, \qquad \vartheta \equiv \begin{Bmatrix} \vartheta_2 \\ \vartheta_3 \end{Bmatrix}. \tag{67, 68}$$

In equations (65) and (68), $\bar{M}^{22}$ and ϑ_2, for instance, are matrices which consist of elements $\bar{M}_{ij}^{22}$ and ϑ_{2j} respectively. The sub-matrices appearing in equation (67) are defined as follows:

$$\begin{aligned} \bar{K}^{22} \equiv [&\bar{K}^{B2} - (c_{31}^2 + c_{33}^2)\gamma^2\bar{M}^{22} \\ &+ \delta\gamma^2(c_{33}c_{22} - c_{32}c_{23})(\bar{K}^{GA2} + \alpha\bar{K}^{GC2}] \\ &+ (c_{32}^2 + c_{33}^2)\gamma^2(\bar{K}^{GB2} + \alpha\beta\bar{K}^{GC2})], \end{aligned} \tag{69}$$

$$\bar{K}^{23} \equiv [\bar{K}^{B23} + c_{33}c_{32}\gamma^2\bar{M}^{23}], \tag{70}$$

$$\bar{K}^{32} \equiv [\bar{K}^{B32} + c_{32}c_{33}\gamma^2\bar{M}^{32}], \tag{71}$$

$$\begin{aligned} \bar{K}^{33} \equiv [&\bar{K}^{B3} - (c_{31}^2 + c_{32}^2)\gamma^2\bar{M}^{33} \\ &+ \delta\gamma^2(c_{33}c_{22} - c_{32}c_{23})(\bar{K}^{GA3} + \alpha\bar{K}^{GC3}] \\ &+ (c_{32}^2 + c_{33}^2)\gamma^2(\bar{K}^{GB3} + \alpha\beta\bar{K}^{GC3})]. \end{aligned} \tag{72}$$

Equation (64) can be transformed into the following equation:

$$\mathbf{M}^*\dot{\eta} + \mathbf{K}^*\eta = \mathbf{0}. \tag{73}$$

The matrices constituting the above equation are defined as follows:

$$\mathbf{M}^* \equiv \begin{bmatrix} \mathbf{M} & \mathbf{0} \\ \mathbf{0} & \mathbf{I} \end{bmatrix}, \qquad \mathbf{K}^* \equiv \begin{bmatrix} \mathbf{C} & \mathbf{K} \\ -\mathbf{I} & \mathbf{0} \end{bmatrix}, \tag{74, 75}$$

$$\eta \equiv \begin{Bmatrix} \dot{\vartheta} \\ \vartheta \end{Bmatrix}, \tag{76}$$

where $\mathbf{I}$ represents an identity matrix. For the complex modal analysis, it is assumed that η is a harmonic function of τ expressed as

$$\eta = \mathrm{e}^{\lambda\tau}\Theta, \tag{77}$$

where λ is the complex eigenvalue and Θ is the corresponding complex mode shape. Substituting equation (77) into equation (73), the following equation is obtained:

$$\lambda\mathbf{M}^*\Theta + \mathbf{K}^*\Theta = \mathbf{0}. \tag{78}$$

From the complex eigenvalues obtained from equation (78), the natural frequencies can be obtained.

3. NUMERICAL RESULTS

Figure 4 shows lowest four dimensionless natural frequencies of a rotating blade that converge rapidly as the number of modes increases. A typical set of dimensionless parameters used for the simulation are shown in the figure. The natural frequencies obtained by using nine modes for each bending deflection are compared with their correspondents obtained by using 10 modes, and it is found that the maximum difference is approximately 0·14%, which may be presumed to be sufficiently small. Therefore, all the numerical results presented hereinafter are obtained by using 10 modes for each bending deflection. In other words, 20 modes are used for the numerical results obtained in this study.

First of all, the accuracy of the present modelling method needs to be confirmed. In Table 1, lowest two natural frequencies of a pre-twisted rotating blade are given. The dimensionless parameters used for the numerical results are shown in the table. All the dimensionless parameters except those shown in the table are zero. The results obtained by using the present modelling method are compared with those obtained by using the plate

TABLE 1

Comparison of natural frequencies ($x = 1/400$, $\theta_0 = 30^\circ$, $\delta = 2/3$)

		First	Second
$\gamma = 0{\cdot}0000$	Reference [13]	0·1766	1·0001
	Present	0·1763	0·9825
$\gamma = 0{\cdot}0882$	Reference [13]	0·2217	1·0273
	Present	0·2200	1·0203
$\gamma = 0{\cdot}1763$	Reference [13]	0·3166	1·1321
	Present	0·3157	1·1253
$\gamma = 0{\cdot}2645$	Reference [13]	0·4277	1·2852
	Present	0·4288	1·2796

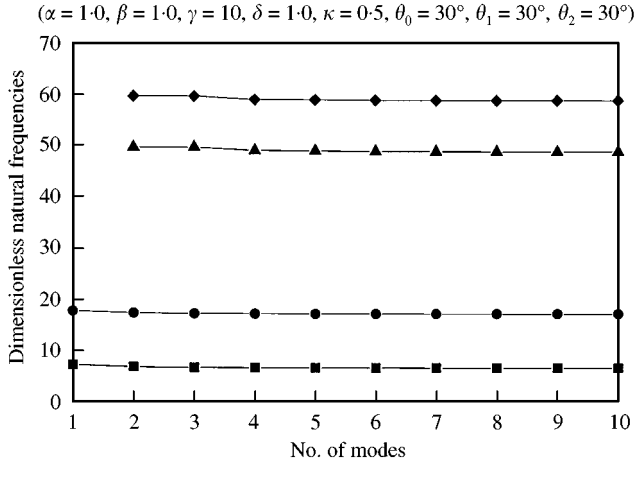

Figure 4. Convergence of natural frequencies: —◆—, fourth natural frequency; —▲—, third natural frequency; —●—, second natural frequency; —■—, first natural frequency

TABLE 2

Comparison of natural frequencies ($\alpha = 1{\cdot}0$, $\beta = 1{\cdot}0$, $x = 1{\cdot}0$)

	First natural frequency		Second natural frequency	
γ	Present	Reference [6]	Present	Reference [6]
0	1·5573	1·5573	16·2527	16·2500
1	1·9017	1·9017	16·7595	16·7570
2	2·6696	2·6696	18·1932	18·1910
3	3·5823	3·5823	20·3524	20·3504
4	4·5429	4·5429	23·0246	23·0229
5	5·5219	5·5218	26·0431	26·0415
6	6·5091	6·5090	29·2933	29·2917
7	7·5007	7·5005	32·7002	32·6984
8	8·4947	8·4945	36·2156	36·2134
9	9·4903	9·4899	39·8079	39·8048
10	10·4870	10·4864	43·4561	43·4517

theory (see reference [13]). The maximum difference between the two results is less than 1·5%. It can be found that the natural frequencies obtained by the present modelling method are generally lower than those obtained in reference [13]. Thus, the present modelling method provides more accurate results.

In Table 2, the results of flapwise bending vibration analysis of a rotating beam with tip mass are given. The dimensionless parameters employed for the numerical results except those shown in the table are zero. The results obtained by using the present modelling method are compared with those introduced in reference [6]. As observed in the table, the two results are found to be almost identical (showing only 0·02% maximum difference).

In Figures 5 and 6, the effects of the concentrated mass and the taper angle on the first natural frequency are shown. With taper angle 30°, the first natural frequency increases as the angular speed increases. It is also shown that the first natural frequency loci are lowered as the concentrated mass ratio increases. In Figure 6, where the taper angle is given 60°

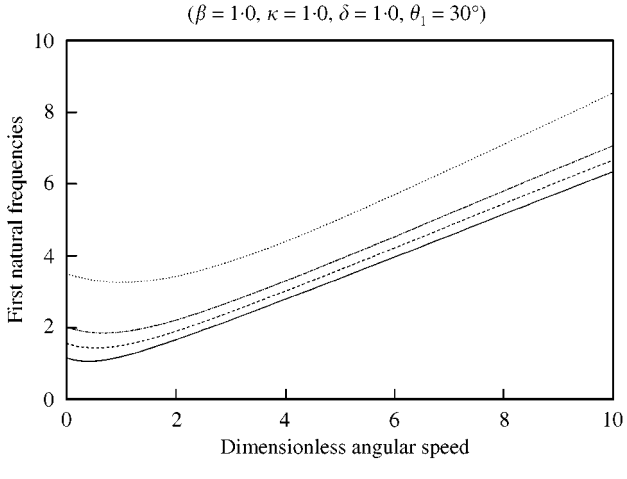

Figure 5. The effect of concentrated mass ratio on the first natural frequency loci (with a taper angle for increasing loci): · · · ·, $\alpha = 0{\cdot}0$; – · – · –, $\alpha = 0{\cdot}5$; - - - - - -, $\alpha = 1{\cdot}0$; ——, $\alpha = 2{\cdot}0$.

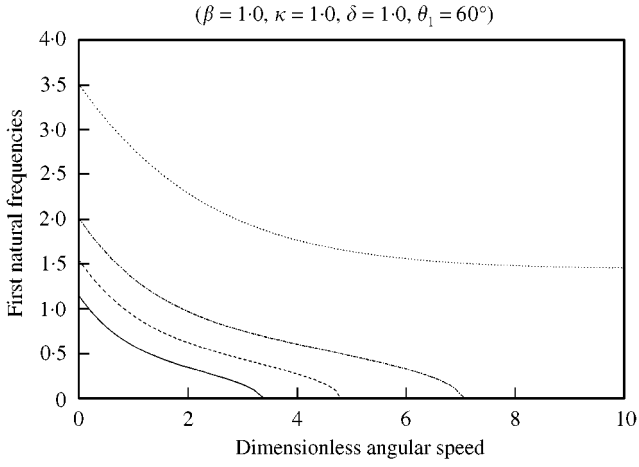

Figure 6. The effect of concentrated mass ratio on the first natural frequency loci (with a taper angle for decreasing loci): · · · ·, $\alpha = 0{\cdot}0$; – · – · – · –, $\alpha = 0{\cdot}5$; - - - - - -, $\alpha = 1{\cdot}0$; ——, $\alpha = 2{\cdot}0$.

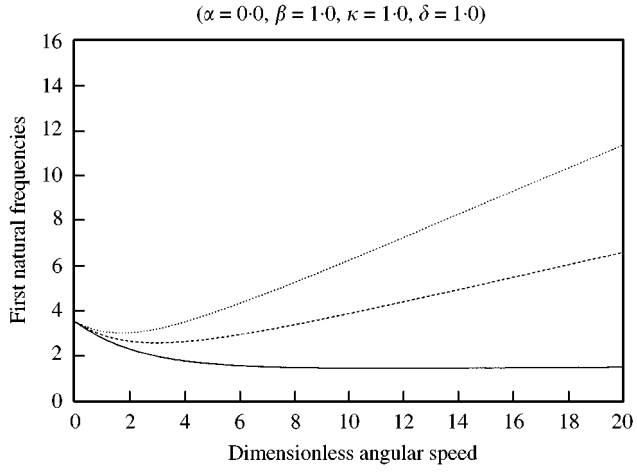

Figure 7. The effect of taper angle on the first natural frequency increasing rate (with no tip mass): · · · · ·, $\theta_1 = 40°$; - - - - -, $\theta_1 = 50°$; ——, $\theta_1 = 60°$.

instead of 30°, the first natural frequency decreases as the angular speed increases. The zero natural frequencies shown in the figure represent the dynamic buckling of the blade due to the centrifugal inertial force. From Figures 5 and 6, one may speculate that there exists a taper angle with which the first natural frequency remains constant even if the angular speed increases. Figure 7 shows the variation of the first natural frequency versus angular speed ratio γ with several taper angles. As shown in the figure, the first natural frequency remains almost constant with the taper angle with which the first natural frequency remains constant changes as the concentrated mass ratio changes (Figure 8).

The effect of the location of concentrated mass on the first natural frequency with zero angular speed is shown in Figure 9. As can be easily speculated, the first natural frequency decreases monotonically as the concentrated mass moves out to the free end. Since no centrifugal inertia force occurs in this case, the taper angle does not affect the natural frequencies. When the blade rotates, however, the centrifugal inertia force occurs and the

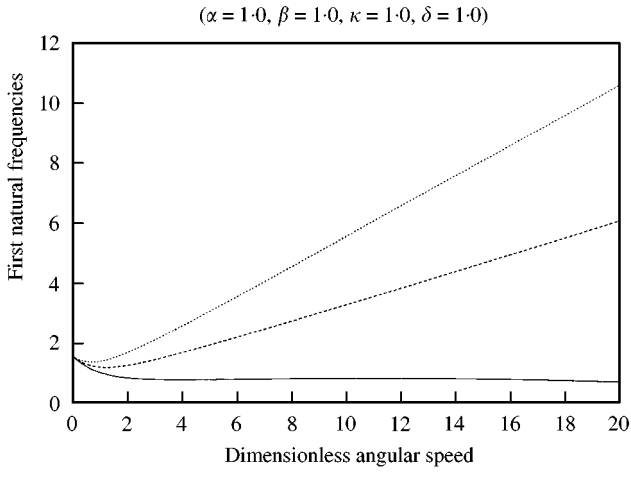

Figure 8. The effect of taper angle on the first natural frequency increasing rate (with a tip mass): ····, $\theta_1 = 35°$; - - - - -, $\theta_1 = 45°$; ——, $\theta_1 = 55°$.

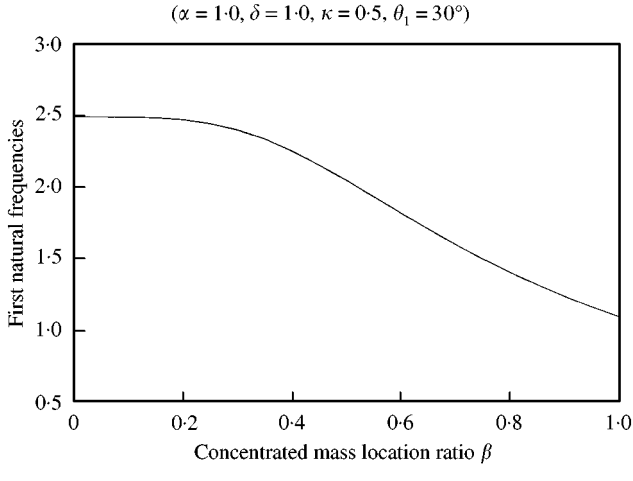

Figure 9. The effect of the location of concentrated mass on the first natural frequency loci (with zero angular speed).

taper angle does affect the natural frequencies. Figure 10 shows the effects of the location of concentrated mass and the taper angle on the first natural frequency with a non-zero angular speed ($\gamma = 10$). As shown in the figure, the first natural frequency increases to some extent and then decreases as the concentrated mass moves out to the free end. The effect of the taper angle on the natural frequency is also shown in the figure. As the taper angle increases, the loci of the first natural frequency are lowered.

In Figure 11, the effect of the magnitude of the concentrated mass on the first natural frequency is exhibited. All the numerical values for the dimensionless parameters except the ones shown in the figure are set to zero. The figure shows that the variation of natural frequency increases as the magnitude of the concentrated mass increases. Thus, the first natural frequency of the rotating blade can be varied by changing the location and the magnitude of the concentrated mass.

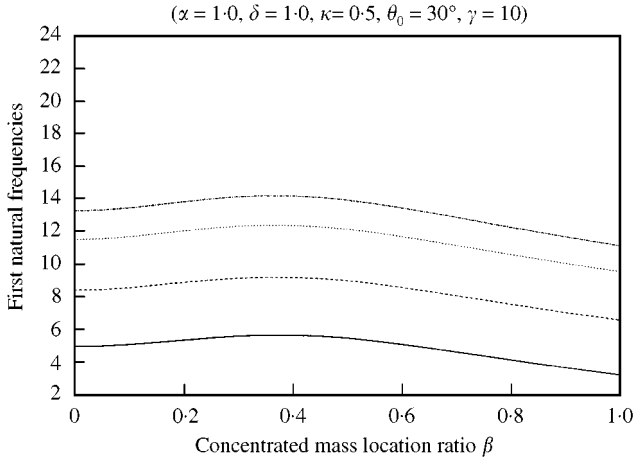

Figure 10. The effect of the location of the concentrated mass on the first natural frequency loci (with non-zero angular speed): · · · ·, $\theta_1 = 0°$; · · · · · ·, $\theta_1 = 15°$; - - - - -, $\theta_1 = 30°$; ——, $\theta_1 = 45°$.

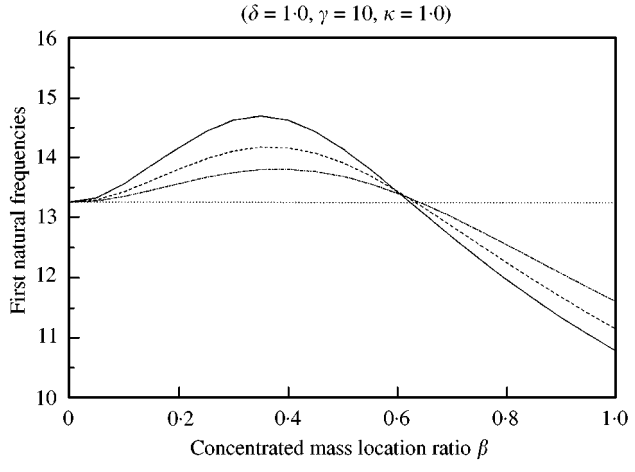

Figure 11. Concentrated mass location effect on the first natural frequency: · · · ·, $\alpha = 0{\cdot}0$; – · – · – · –, $\alpha = 0{\cdot}5$; - - - - - -, $\alpha = 1{\cdot}0$; ——, $\alpha = 2{\cdot}0$.

Figure 12 shows lowest two natural frequencies of a pre-twisted blade. When the taper angle is zero, the two loci cross. With a small non-zero taper angle, however, the two loci veer rather than cross. The veering phenomena were previously observed and discussed in other vibration problems (see, for instance, reference [16]). As the taper angle increases, the gap between the two natural frequency loci increases.

When the angular speed and one of the natural frequencies of rotating blades match (as shown in Figure 13), resonance occurs. Such an angular speed is usually called the tuned angular speed. Catastrophic failures are often caused at the tuned angular speed during the operation of rotating blades. Thus, the tuned angular speed needs to be calculated for the design of a rotating blade. The tuned angular speeds are tabulated in Tables 3 and 4. The two tables (for different area moment of inertia ratios) show the variation of the tuned

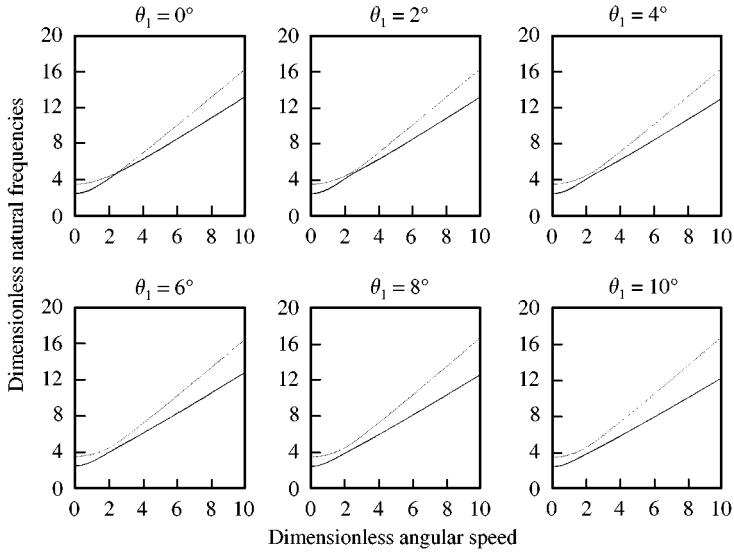

Figure 12. Veering phenomena occurring in a pre-twisted rotating blade with taper angles ($\delta = 1{\cdot}0$, $\kappa = 0{\cdot}5$, $\theta_0 = 5°$): - - - -, first; ——, second.

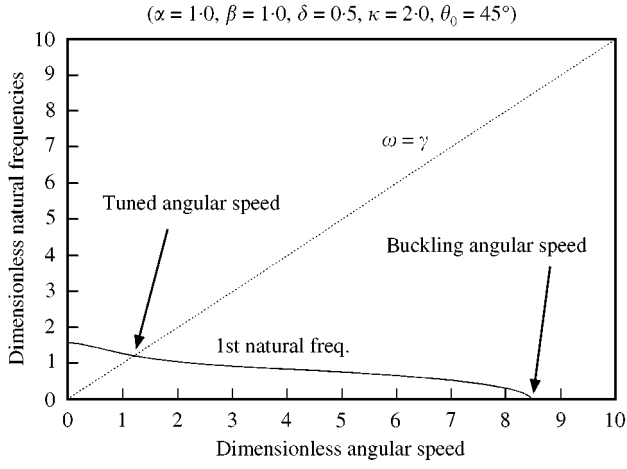

Figure 13. Tuned angular speed and buckling angular speed.

angular speed caused by the variations of the hub radius, the pre-twist angle, and the taper angle.

4. CONCLUSION

The equations of motion for the vibration analysis of rotating blades, which have a pre-twisted cross-section, arbitrary orientation, and a concentrated mass in arbitrary location, are derived. The equations of motion are transformed into a dimensionless form by employing dimensionless variables and several dimensionless parameters representing the concentrated mass and its location, the angular speed, the hub radius, and the principal

TABLE 3

Tuned angular speed versus hub radius ratio, pre-twist angle, and taper angle ($\alpha = 1$, $\beta = 1$, $x = 0{\cdot}5$)

δ	θ_1 (deg)	$\theta_0 = 0^\circ$	$\theta_0 = 15^\circ$	$\theta_0 = 30^\circ$	$\theta_0 = 45^\circ$
0·0	0	1·7202	1·7172	1·7085	1·6945
	30	1·0182	1·0174	1·0151	1·0113
	60	0·7091	0·7090	0·7086	0·7080
0·1	0	1·8633	1·8606	1·8525	1·8394
	30	1·0535	1·0526	1·0502	1·0463
	60	0·7167	0·7166	0·7162	0·7156
0·2	0	2·0458	2·0433	2·0359	2·0238
	30	1·0920	1·0912	1·0886	1·0846
	60	0·7246	0·7244	0·7240	0·7234
0·3	0	2·2881	2·2858	2·2791	2·2682
	30	1·1344	1·1335	1·1309	1·1267
	60	0·7327	0·7325	0·7321	0·7314
0·4	0	2·6273	2·6254	2·6195	2·6100
	30	1·1814	1·1805	1·1777	1·1734
	60	0·7410	0·7408	0·7404	0·7397
0·5	0	3·1393	3·1377	3·1329	3·1250
	30	1·2338	1·2328	1·2300	1·2255
	60	0·7496	0·7494	0·7489	0·7482

TABLE 4

Tuned angular speed versus hub radius ratio, pre-twist angle, and taper angle ($\alpha = 1$, $\beta = 1$, $x = 2$)

δ	θ_1 (deg)	$\theta_0 = 0^\circ$	$\theta_0 = 15^\circ$	$\theta_0 = 30^\circ$	$\theta_0 = 45^\circ$
0·0	0	1·7202	1·7224	1·7288	1·7391
	30	1·2763	1·2770	1·2791	1·2824
	60	0·9788	0·9789	0·9793	0·9798
0·1	0	1·8633	1·8656	1·8723	1·8831
	30	1·3195	1·3202	1·3222	1·3256
	60	0·9892	0·9894	0·9897	0·9902
0·2	0	2·0458	2·0482	2·0553	2·0665
	30	1·3668	1·3675	1·3696	1·3729
	60	1·0000	1·0001	1·0004	1·0009
0·3	0	2·2881	2·2906	2·2978	2·3093
	30	1·4192	1·4199	1·4219	1·4251
	60	1·0111	1·0112	1·0115	1·0119
0·4	0	2·6273	2·6298	2·6369	2·6484
	30	1·4773	1·4780	1·4800	1·4832
	60	1·0225	1·0226	1·0228	1·0232
0·5	0	3·1393	3·1416	3·1484	3·1591
	30	1·5424	1·5430	1·5450	1·5481
	60	1·0342	1·0343	1·0346	1·0349

area moment of inertia ratio, the pre-twist angle, and the taper angle are identified. The effects of some dimensionless parameters on the vibration characteristics of the rotating blade are investigated through numerical study. Combinatory effects among dimensionless parameters are also exhibited in this study.

ACKNOWLEDGMENTS

This research was supported by Center of Innovative Design Optimization Technology (iDOT), Korea Science and Engineering Foundation.

REFERENCES

1. R. SOUTHWELL and F. GOUGH 1921 *British A.R.C. Reports and Memoranda*, *No*. 766. The free transverse vibration of airscrew blades.
2. M. SCHILHANSL 1958 *Journal of Applied Mechanical Transactions of the American Society of Mechanical Engineers* **25**, pp. 28–30. Bending frequency of a rotating cantilever beam.
3. S. PUTTER and H. MANOR 1978 *Journal of Sound and Vibration* **56**, 175–185. Natural frequencies of radial rotating beams.
4. H. BAUER 1980 *Journal of Sound and Vibration* **72**, 177–189. Vibration of a rotating uniform beam.
5. S. HOA 1979 *Journal of Sound and Vibration* **67**, 369–381. Vibration of a rotating beam with tip mass.
6. A. WRIGHT, C. SMITH, R. THRESHER and J. WANG 1982 *Journal of Applied Mechanics* **49**, 197–202. Vibration modes of centrifugally stiffened beams.
7. Y. KUO, T. WU and S. LEE 1994 *Computers and Structure*, **22**, 229–236. Bending vibration of a rotating non-uniform beam with tip mass and an elastically restrained root.
8. T. YOKOYAMA 1988 *International Journal of Mechanical Science* **30**, 743–755. Free vibration characteristics of rotating Timoshenko beams.
9. K. SUBRAHMANYAM, K. KAZA, G. BROWN and C. LAWRENCE 1987 *Journal of Aircraft* **24**, 342–352. Non-linear vibration and stability of rotating pre-twisted, preconed blades including Coriolis effects.
10. H. YOO and S. SHIN 1998 *Journal of Sound and Vibration* **212**, 807–828. Vibration analysis of rotating cantilever beams.
11. A. LEISSA 1981 *Applied Mechanics Reviews* **34**, 629–635. Vibration aspects of rotating turbomachinery blades.
12. J. RAO 1987 *Shock Vibration Digest* **19**, 3–10. Turbomachine blade vibration.
13. V. RAMAMURTI and R. KIELB 1984 *Journal of Sound and Vibration* **97**, 429–449. Natural frequencies of twisted rotating plates.
14. T. KANE and D. LEVINSON 1985 *Dynamics*: *Theory and Application*. New York: McGraw-Hill.
15. H. YOO, R. RYAN and R. SCOTT 1995 *Journal of Sound and Vibration* **181**, 261–278. Dynamics of flexible beams undergoing overall motions.
16. A. LEISSA 1974 *Journal of Applied Mathematics and Physics* (*ZAMP*) **25**, 99–111. On a curve veering aberration.